Interaction of Samarium with Nickel and Arsenic: Phase Diagram and Structural Chemistry

Volodymyr Babizhetskyy[a], Roland Guérin[b], and Arndt Simon[a]

[a] Max-Planck-Institut für Festkörperforschung, Heisenbergstraße 1, D-70569 Stuttgart, Germany
[b] Laboratoire de Chimie du Solide et Inorganique Moléculaire, UMR CNRS 6511, Université de Rennes 1, Institut de Chimie, Campus de Beaulieu, Avenue du Général Leclerc, F-35042 Rennes Cedex, France

Reprint requests to V. Babizhetskyy. E-mail: v.babizhetskyy@fkf.mpg.de

Z. Naturforsch. **61b,** 733 – 740 (2006); received February 15, 2006

Dedicated to Professor Wolfgang Jeitschko on the occasion of his 70th birthday

Solid-state phase equilibria in the Sm-Ni-As system have been established using X-ray diffraction, scanning electron microscopy and electron probe microanalysis. The samarium-poor region up to 33 at. % Sm was studied at 1170 K, whereas the Sm-rich corner, due to the generally lower melting points, was investigated at 770 K. Six ternary compounds were isolated, among which two have been structurally characterized. The hexagonal structure of SmNiAs (SrPtSb-type) was solved from X-ray single crystal data: space group $P\bar{6}m2$, $a = 4.0904(3)$, $c = 3.8957(4)$ Å, $Z = 1$, $R1 = 0.0221$, $wR2 = 0.0224$ for 134 unique reflections with $I_o > 2\sigma(I_o)$ and 9 variable parameters. The crystal structure of $Sm_6Ni_{15}As_{10}$ ($Tb_6Ni_{15}As_{10}$-type) was determined from X-ray powder diffraction data: full profile refinement, space group $P6_3/m$, $a = 17.0632(4)$, $c = 3.9526(1)$ Å, $Z = 2$, $R_B = 0.079$, $R_p = 0.138$.

Key words: Samarium Nickel Arsenide, Solid-State Phase Equilibria, Crystal Structure

Introduction

The search for new ternary pnictides predicted from several structural models recently led to a systematic study of ternary phase diagrams, especially of phosphides and arsenides. Numerous ternary *Ln*-*T*-P phase diagrams (*Ln* = lanthanoid) were established with *T* = Cr, Fe, Ni, Co, Cu [1]. The isothermal section of the Sm-Ni-P system was constructed at 1070 and 870 K using X-ray phase analysis [2]. Eleven ternary samarium nickel phosphides were found, and most of them were structurally characterized. Neither solid solutions based on binary compounds nor homogeneity ranges of ternary phases were detected.

The phase relations in the general *Ln*-Ni-As systems were not studied in sufficient detail so far. Recently, we reported on the solid-state phase equilibria in the ternary phase diagrams with *Ln* = La, Ce [3]. The crystal structures of the Ce-containing compounds were determined from X-ray single crystal data, except CeNiAs which was solved from X-ray powder data [3], and the other ternary lanthanoid nickel arsenides were found to be isotypic from experimental X-ray powder patterns. Beyond, three new series of ternary lanthanoid nickel arsenides were synthesized, *Ln*NiAs (SrPtSb or YbPtP-type respectively) (*Ln* = La to Tm) [1, 3, 4], $Ln_{20}Ni_{42}As_{31}$ ($Sm_{20}Ni_{42}P_{31}$-type) (*Ln* = La to Dy) [3, 5], $Ln_3Ni_7As_5$ ($Ce_3Ni_7As_5$-type) (*Ln* = La to Sm) [3, 6], and with La a new compound $LaNi_5As_3$ was identified with its own structure type [7].

Most of the ternary lanthanoid nickel arsenides have a hexagonal structure and a metal/metalloid ratio equal or close to 2. Structural relationship of the intermetallic compounds exhibiting such a ratio have been previously reported, applying various models proposed by different authors [1, 8, 9]. As an example, the series with the general chemical formula $R_{n(n-1)}T_{(n+1)(n+2)}X_{n(n+1)+1}$ (R = Zr or *Ln*; T = 3d or 4d transition metal; X = P, As and n = integer) contains the Fe_2P, $Zr_2Fe_{12}P_7$, $Zr_6Ni_{20}P_{13}$, $(La, Ce)_{12}Rh_{30}P_{21}$, $Sm_{20}Ni_{42}P_{31}$, and $Tb_{15}Ni_{28}P_{21}$ structural types with $n = 1$ to 6, while the limiting SrPtSb-type structure results when n reaches infinity [1].

In order to pursue our systematic research on the *Ln*-Ni-As phases, we focused on the solid-state phase

equilibria in the ternary Sm-Ni-As phase diagram. In addition to the structural series containing samarium which have been mentioned above, a new series $Ln_6Ni_{15}As_{10}$ ($Tb_6Ni_{15}As_{10}$-type) (*Ln* = Y, Sm, Gd, Tb, Dy) has recently been reported [10]. Hence, the presentation of the isothermal sections of the ternary Sm-Ni-As phase diagram at 1170 K (concentration range 0 – 33 at. % Sm) and 770 K (> 33 at. % Sm), crystallographic data of all the ternary compounds and the structure determinations for two of them, $Sm_6Ni_{15}As_{10}$ and SmNiAs, are the subject of this work.

Experimental Determination of the Sm-Ni-As Phase Diagram

Experimental details

Polycrystalline samples were prepared from pure elements: nickel and amorphous β-As as powders, rare earth metals as ingots, all with minimum purity 99.99% and supplied by Strem Chemicals. Stoichiometric amounts of powders and freshly filed chips of samarium were mixed and pressed into pellets. A small excess of arsenic ($\sim$ 0.1 g) was added to compensate for evaporation losses during arc-melting. Prior to the melting performed on a water-cooled copper hearth under a purified argon atmosphere with a Ti alloy as a getter, the pellets were pre-reacted in evacuated silica tubes by gradually heating them to 870 K, kept at this temperature for 2 days and slowly cooled to room temperature. To ensure homogeneity during arc-melting, the samples were turned over and re-melted several times. Finally, to reach thermodynamic equilibrium, the so-obtained samples were again sealed in evacuated silica tubes, which were heated for 1 month at 1170 K (within the concentration range 0 – 33 at. % Sm) and subsequently quenched in cold water. For the arsenic-rich samples (> 33.3 at. % As) at 770 K, all the syntheses and re-annealings were carried out in furnace heated ampoules.

The samples were characterized by X-ray diffraction, metallographic and microprobe analysis. Lattice parameters were derived from the least-square refinements on X-ray powder diffractometer data (Image Plate Huber G 670, $8^\circ \leq 2\theta \leq 100^\circ$, step size 0.005° with monochromated Cu-$K_{\alpha 1}$ radiation). Elemental germanium (99.9999%, a_{Ge} = 5.657905 Å) served as the internal standard. The lattice parameters of the Sm-Ni-As phases are listed in Table 2. X-ray powder diffraction patterns for the full profile refinement of the ternary compound $Sm_6Ni_{15}As_{10}$ were collected on a powder diffractometer STOE STADI P with monochromated Mo-$K_{\alpha 1}$ radiation ($8^\circ \leq 2\theta \leq 75^\circ$, step size 0.1°, measurement time per step: 200 s).

For analyses half of each sample was embedded in epoxy resin, polished down to 0.25 mm diamond grade and coated with either a gold or graphite thin layer to obtain a good surface conductivity. Electron probe microanalyses (EPMA) were performed by energy dispersive spectroscopy (EDS) of X-rays using scanning electron microscopy (Jeol JSM-6400). The compositions were checked against the diffraction data to identify the phases present in each sample in order to establish the ternary phase diagram.

Small plate-like single crystals of SmNiAs (metallic lustre, unreactive towards air) were isolated by crushing the samples. Single-crystal intensity data were collected at ambient temperature applying a Nonius Kappa CCD X-ray area-detector diffractometer with graphite-monochromatized Mo-$K_{\alpha 1}$ radiation ($\lambda = 0.71073$ Å). Data collection strategy was performed with the help of the program COLLECT [11], and reflections were corrected using the program DENZO of the Kappa CCD software package [12]. Structures were solved by direct methods (SIR 97) [13] and least-squares refinements, difference Fourier syntheses were run with the SHELXL-97 program package (full-matrix least-squares on F^2) with anisotropic atomic displacements for all atoms [14]. Owing to the small size of the single crystal, no absorption correction was necessary. The program DIAMOND [15] was used for the drawings of the structural units.

Further details of the crystal structure investigation are available from the Fachinformationszentrum Karlsruhe, D-76344 Eggestein-Leopoldshafen (Germany) by quoting the registry No. CSD-416244.

Constituent binaries

The initial informations concerning the binary boundary systems Sm-Ni, Sm-As and Ni-As have been collected from reference books [16, 17]. Crystallographic data on the phases belonging to these binary systems are listed in Table 1. According to the phase diagram of the Sm-Ni system, the binary compounds SmNi and $SmNi_5$ melt congruently while the others, Sm_3Ni, $SmNi_2$, $SmNi_3$, Sm_2Ni_7, Sm_5Ni_{19} and Sm_2Ni_{17}, are formed by peritectic reactions. Sm_2Ni_7 displays two polymorphic modifications, the high temperature form belonging to the Ce_2Ni_7 type and the low temperature form to the Gd_2Co_7 type [18]. Structural data for Sm_5Ni_{19} are more complex since four polymorphic modifications derived from the $CaCu_5$ type have been deduced from electron diffraction patterns [19]. In contrast, only four binary phases occur in the Ni-As system, $NiAs_2$ (with an $\alpha \leftrightarrow \beta$ transformation at about 860 K) and NiAs, $Ni_{11}As_8$ and Ni_5As_2. Only one binary arsenide SmAs (rocksalt type) is mentioned in the Sm-As system, however another one reported [20 – 22], Sm_4As_3 (anti-Th_3P_4 type), has never been observed during our own investigations, which confirm other previous studies [23, 24].

In our investigations, all binary phases previously reported, except for Sm_2Ni_{17}, Sm_5Ni_{19} and Sm_4As_3, have

Compound	Space group	Structure type	Lattice parameters (Å)			Ref.
			a	*b*	*c*	
Sm_2Ni_{17}	$P6_3/mmm$	Th_2Ni_{17}	8.471		8.049	[17]
$SmNi_5$	$P6/mmm$	$CaCu_5$	4.926		3.980	[17]
Sm_2Ni_7 (LT)	$R3m$	Gd_2Co_7	4.969		36.53	[18]
Sm_2Ni_7 (HT)	$P6_3/mmc$	Ce_2Ni_7	4.969		24.35	[18]
Sm_5Ni_{19}	$P6_3/mmc$	—	5.0		65.0	[19]
	$P\bar{6}m2$	—	5.0		97.0	[19]
	$R\bar{3}m$	—	5.0		150.0	[19]
	$R\bar{3}m$	—	5.0		190.0	[19]
$SmNi_3$	$R3m$	$NbBe_3$	5.00		24.59	[17]
$SmNi_2$	$Fd\bar{3}m$	$MgCu_2$	7.2247			[17]
Sm_3Ni	$Pnma$	Fe_3C	6.99	9.72	6.37	[17]
Ni_5As_2	$P6_3cm$	Ni_5As_2	6.815		12.506	[17]
$Ni_{11}As_8$	$P4_12_12$	$Ni_{11}As_8$	6.872		21.821	[17]
NiAs	$P6_3/mmc$	NiAs	3.619		5.044	[17]
α-$NiAs_2$	$Pbca$	$NiAs_2$	5.770	5.838	11.419	[17]
β-$NiAs_2$	$Pnm\bar{m}$	FeS_2	4.7582	5.794	3.544	[17]
SmAs	$Fm\bar{3}m$	NaCl	5.921			[17]
Ni	$Fm\bar{3}m$	Cu	3.5236			[17]

Table 1. Crystallographic data of binary phases and their structure types in the Sm-Ni, Ni-As and Sm-As systems.

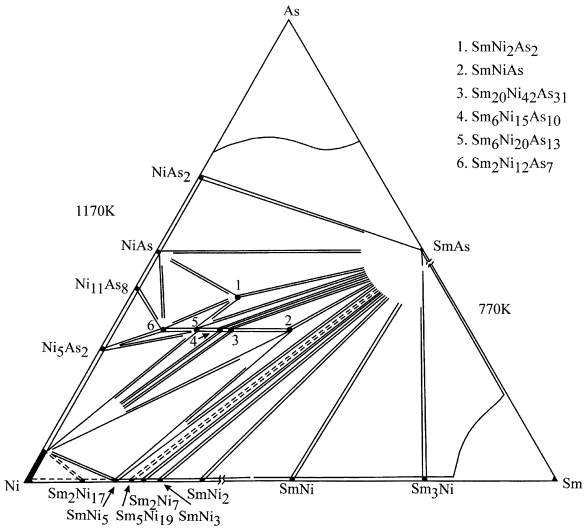

Fig. 1. Sm-Ni-As isothermal section at 1170 K (0–33 at. % Sm) and 770 K (33–80 at. % Sm) with labelling phases.

been found, and no homogeneity ranges were detected. The solubility of As in Ni was found to be about 8.5% at 1170 K.

Ternary Sm-Ni-As system

On the basis of the binary compounds mentioned above, the isothermal section of the ternary phase diagram Sm-Ni-As was constructed at 1170 K (0–33 at. % Sm) and 770 K (33–80 at. % Sm), respectively. The highest As-rich (> 70 at. % As) and Sm-rich (> 80 at. % Sm) regions could not be studied owing to the vapour pressure of elemental arsenic and samarium.

The Sm-Ni-As ternary phase diagram was derived using X-ray powder patterns of 35 samples and microprobe analyses of about 15 representative samples (Fig. 1). In the concentration region 0–33 at. % Sm, the formation and phase equilibria of six ternary phases, $SmNi_2As_2$, SmNiAs, $Sm_{20}Ni_{42}As_{31}$, $Sm_6Ni_{15}As_{10}$, $Sm_6Ni_{20}As_{13}$ and $Sm_2Ni_{12}As_7$ were established. Owing to the absence of the binary alloy Sm_2Ni_{17} (probably due to too low annealing temperature), the occurrence of a tri-phasic region $Ni_{0.915}As_{0.085}$-$SmNi_5$-SmNiAs was found. With the exception of $Sm_2Ni_{12}As_7$, all the ternary phases were found in thermodynamic equilibrium with both the monoarsenide SmAs and the solid solution $Ni_{1-x}As_x$ ($x = 0.085$). In contrast, no ternary phase in the Sm-rich part of the phase diagram (33–80 at. % Sm) at 770 K was detected. In fact, only three-phase regions defined by SmAs and Sm-rich alloys, like SmNi and Sm_3Ni, were observed.

The crystallographic characteristics of the ternaries in the Sm-Ni-As system are listed in Table 2. It is worth noting that, at the reaction temperature of 1170 K, $SmNi_2As_2$ only crystallizes as $CaBe_2Ge_2$ not as $ThCr_2Si_2$ type, corresponding to high and low-temperature structures, respectively. No evidence for a ternary compound $Sm_3Ni_7As_5$ ($Ce_3Ni_7As_5$-type structure) [6, 25, 26] at the temperature of investigation has been found.

Crystal structure of $Sm_6Ni_{15}As_{10}$

The structure of $Sm_6Ni_{15}As_{10}$ was determined from Rietveld-type profile refinement using the WinPLOTR and Fullprof programs [30, 31], starting from the atomic coordinates of isotypic $Tb_6Ni_{15}As_{10}$ [10]. The final refinement shows good agreement between observed and calculated diffraction patterns, see Fig. 2, except for some traces of

Compound	Space group	Structure type	Lattice parameters (Å) *a*	*c*	Ref.
1 $SmNi_2As_2$	$I4/mmm$	$ThCr_2Si_2$	4.0549(2)	9.5411(8)	*
			4.021	9.854	[25, 26]
2 SmNiAs	$P\bar{6}m2$	SrPtSb	4.0904(3)	3.8957(4)	**
			4.0950(4)	3.8956(6)	*
			4.090	3.939	[3]
3 $Sm_{20}Ni_{42}As_{31}$	$P6_3/m$	$Sm_{20}Ni_{42}P_{31}$	21.079(2)	3.9575(1)	*
			21.078	3.956	[5]
4 $Sm_6Ni_{15}As_{10}$	$P6_3/m$	$Tb_6Ni_{15}As_{10}$	17.0632(4)	3.9525(1)	*
			17.074	3.942	[10]
5 $Sm_6Ni_{20}As_{13}$	$P\bar{6}$	$Zr_6Ni_{20}P_{13}$	13.147(1)	3.9113(4)	*
			13.146	3.920	[27]
6 $Sm_2Ni_{12}As_7$	$P\bar{6}$	$Zr_2Fe_{12}P_7$	9.3682(6)	3.8518(4)	*
			9.376	3.850	[28, 29]

Table 2. Crystallographic data of ternary compounds in the Sm-Ni-As phase diagram.

* Powder data of our present work; ** single crystal data of our present work.

Table 3. Crystal data of the structure refinement for the $Sm_6Ni_{15}As_{10}$.

Space group Lattice parameters	$P6_3/m$ (No. 176)
a (Å)	17.0632(4)
c (Å)	3.9526(1)
Cell volume, (Å^3)	996.62(4)
Number of atoms in cell	64
Calculated density (g/cm^3)	8.589(1)
Diffractometer	STOE STADI P
Radiation	Mo-$K_{\alpha1}$
Mode of refinement	Full matrix full profile data refinement
Number of atom sites	15
Number of free parameters	42
2ϑ limits	8 – 75
R_{Bragg}, R_p, R_{wp}, R_{exp}	0.079, 0.138, 0.135, 0.098

Table 4. Positional and isotropic thermal parameters for $Sm_6Ni_{15}As_{10}$.

Atom	Position	Occupancy factor	*x*	*y*	*z*	B_{iso}
Sm1	6*h*	1	0.6140(3)	0.4363(3)	1/4	0.20(3)
Sm2	6*h*	1	0.3587(3)	0.2356(3)	1/4	0.20(3)
As1	2*b*	0.12(3)	0	0	0	1.7(5)
As2	2*c*	1	1/3	2/3	1/4	1.3(3)
As3	6*h*	1	0.5354(5)	0.6107(5)	1/4	0.9(3)
As4	6*h*	1	0.5924(5)	0.8679(5)	1/4	0.9(3)
As5	6*h*	1	0.0227(5)	0.2046(6)	1/4	0.9(3)
As6	2*a*	0.18(3)	0	0	1/4	1.7(4)
Ni1	6*h*	1	0.4937(7)	0.7159(8)	1/4	1.1(2)
Ni2	6*h*	1	0.3483(6)	0.0415(7)	1/4	1.1(2)
Ni3	6*h*	1	0.7528(5)	0.9334(6)	1/4	1.1(2)
Ni4	6*h*	1	0.5505(6)	0.9818(7)	1/4	1.1(2)
Ni5	6*h*	0.60(2)	0.9158(7)	0.0569(7)	1/4	1.2(4)
Ni6	6*h*	0.30(4)	0.929(3)	0.044(3)	1/4	1.8(4)
Ni7	6*h*	0.10(5)	0.953(6)	0.025(6)	1/4	2.1(5)

the binary arsenide SmAs detected as impurity during refinement. Crystal data and experimental details are listed in Table 3 and the final atomic and isotropic displacement parameters of $Sm_6Ni_{15}As_{10}$ in Table 4.

A projection of the $Sm_6Ni_{15}As_{10}$ structure along (001) is shown in Fig. 3, together with the typical coordination poly-

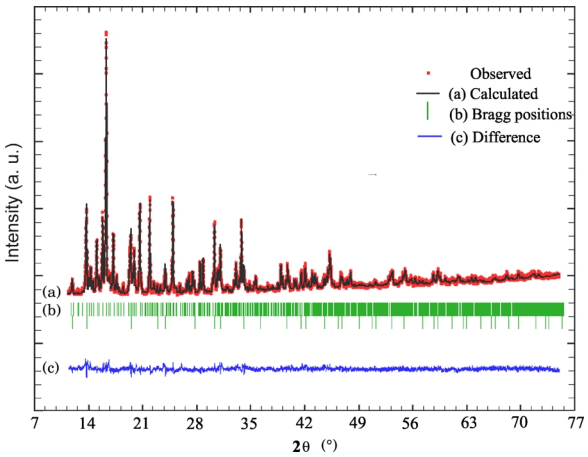

Fig. 2. Comparison of observed and calculated X-ray powder profiles for $Sm_6Ni_{15}As_{10}$.

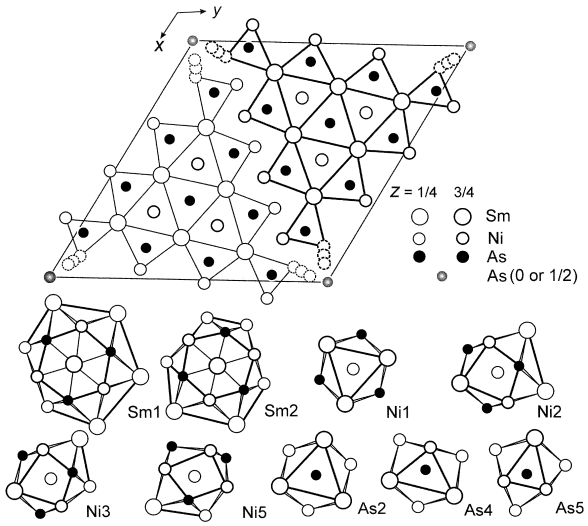

Fig. 3. Crystal structure of $Sm_6Ni_{15}As_{10}$ in a projection on (001). Selected coordination polyhedra of corresponding atoms are emphasized.

Table 5. Selected interatomic distances in the structure of $Sm_6Ni_{15}As_{10}$.

Atoms		δ (Å)	Atoms		δ (Å)
Sm1: –	2As3	2.986(8)	As4: –	2Sm2	3.018(8)
	2Ni1	3.028(9)		2Sm1	3.074(8)
	2As2	3.049(4)			
	2As4	3.074(7)	As5: –	Ni5	2.25(1)
	2Ni4	3.12(1)		2Ni3	2.387(8)
	2Ni1	3.139(9)		Ni3	2.41(1)
	Ni4	3.23(1)		2Ni5	2.445(9)
	Ni2	3.25(1)		Ni2	2.47(1)
	2Sm1	3.9181(1)		2Sm2	3.027(7)
	Sm2	3.967(7)			
	Sm2	4.076(7)	Ni1: –	As3	2.23(1)
	2Sm1	4.077(7)		As4	2.27(1)
				As2	2.42(1)
Sm2: –	2Ni1	2.96(1)		2Sm2	2.96(1)
	2As4	3.018(8)		4Sm1	3.03(1)
	2As5	3.027(9)			
	2As3	3.037(7)	Ni2: –	2As4	2.384(7)
	Ni3	3.14(1)		As3	2.41(1)
	2Ni2	3.16(1)		As5	2.47(1)
	2Ni3	3.204(7)		2Ni3	2.78(1)
	Ni4	3.21(1)		2Ni4	2.77(1)
	Ni2	3.22(1)		2Sm2	3.163(9)
	Ni5	3.29(1)		2Sm1	3.21(1)
	2Sm2	3.9181(1)			
	Sm1	3.967(7)	Ni3: –	As4	2.38(1)
	Sm1	4.076(8)		2As5	2.387(7)
				As5	2.41(1)
As2: –	3Ni1	2.42(1)		Ni5	2.51(1)
	6Sm1	3.049(3)		2Ni5	2.78(1)
				2Ni2	2.78(1)
As3: –	Ni1	2.23(1)		Sm2	3.14(1)
	2Ni4	2.407(8)		2Sm2	3.204(8)
	Ni4	2.41(1)			
	Ni2	2.46(1)	Ni4: –	As4	2.38(1)
	2Sm1	2.986(8)		2As3	2.407(7)
	2Sm2	3.037(7)		As3	2.42(1)
				2Ni2	2.77(1)
As4: –	Ni1	2.28(1)		2Ni4	2.87(1)
	Ni3	2.38(1)		2Sm1	3.118(9)
	Ni4	2.38(1)		Sm2	3.21(1)
	2Ni2	2.384(7)		Sm1	3.23(1)

hedra (CP) of the atoms. The Sm1 and Sm2 atoms exhibit peculiar environments in the form of hexagonal prisms with additional atoms outside the faces, *i. e.* coordination numbers CN = 20. Most of the nickel atoms have CNs from 9 to 12 corresponding to trigonal or orthorhombic prisms with additional arsenic or metal atoms outside the rectangular faces. The surrounding of the atoms denoted as Ni5, Ni6 and Ni7 is more complex due to their close contacts in 6*h* positions as well as low occupancy factors (Table 4). The structure refinement has been performed with constrained split positions (60% Ni5, 30% Ni6 and 10% Ni7). Fig. 3 represents the coordination polyhedron for the Ni5 atom, which exhibits the highest occupancy factor.

Table 6. Crystal data, intensity collection and refinement for SmNiAs.

Empirical formula	SmNiAs
Formula weight [g·mol^{-1}]	283.96
Crystal system	hexagonal
Space group	$P\bar{6}m2$ (No.187)
a [Å]	$a = 4.0904(3)$
c [Å]	$c = 3.8957(4)$
V [Å^3]	56.448(8)
Z, calculated density [g·cm^{-3}]	1; 8.35
Crystal shape	Platelet
Crystal size [mm^3]	$0.004 \times 0.015 \times 0.001$
Linear absorption coefficient [mm^{-1}]	48.2
Refinement limits:	
2θ Limits [deg.]	$4 < \theta < 75$
Data collected	$-6 < h < 6$
	$-6 < k < 5$
	$-6 < l < 5$
Reflections collected	813
Independent reflections	137; ($R_{int} = 0.056$)
Reflections with $I_o > 2\sigma(I_o)$	134; ($R_\sigma = 0.030$)
Variable parameters	9
Refinement	F^2
Final R_1[a] indices [R_1[a] all data]	0.0221 (0.0224)
Weighted wR_2[b] factor [wR_2[b] all data]	0.0571 (0.0574)
Flack parameter	0.1(13)
Goodness-of-fit on F^2	1.05
Min/max [e Å^{-3}]	−3.56/1.05[c]

[a] $R_1(F) = [\Sigma(|F_o| - |F_c|)]/\Sigma|F_o|$; [b] $wR_2(F^2) = [\Sigma[w(F_o^2 - F_c^2)^2/\Sigma[w(F_o^2)^2]]^{1/2}$; $[w^{-1} = \sigma^2(F_o)^2 + (0.030P)^2 + 0.451P]$, where $P = (F_o^2 + 2F_c^2)/3$; [c] Position close to that of the Sm atoms.

All arsenic atoms, except As1 and As6, occupy trigonal prisms formed by the metal atoms, with additional atoms outside the lateral faces, CN = 9. For the As1 and As6 atoms, the coordination polyhedra are more difficult to define. The splitting of the Ni atom position induces also a splitting for As in 0, 0, *z*, which has been refined with two constrained positions, $z = 0$, 1/2 and $z = 1/4$, 3/4, respectively (Table 4). These positions, As1 and As6, are very close to each other ($c/4$) and cannot be occupied at the same time. Such a metalloid disorder on 0, 0, *z* coupled to that of the surrounding metal atoms is frequently found in binary or ternary pnictides having hexagonal symmetry and a metal/metalloid ratio equal or close to 2. Numerous examples can be found, *e. g.* on $Cr_{12}P_7$, $Rh_{12}As_7$, $La_6Rh_{32}P_{17}$, $Ho_{20}Ni_{66}P_{43}$, or $Zr_6Cr_{60}P_{39}$ [1, 9, 32].

Interatomic distances (Table 5) in the structure (not taking into account the distances between atoms with partly occupied positions) are close to the sum of the metallic radii of Sm (1.81 Å) and/or Ni (1.24 Å) and the covalent radius of As (1.18 Å) [33, 34]. The Sm-As distances vary between 2.986(8) and 3.074(7) Å, while those for Ni-As lie between 2.23(1) and 2.47(1) Å, depending on the CNs of the Ni atoms. The same result is observed for the Sm-Ni distances which range from 2.96(1) to 3.29(1) Å.

Table 7. Atomic coordinates and displacement parameters (in Å^2, $U_{23} = U_{13} = 0$) for SmNiAs.

Atom	Wykloff position	x	y	z	U_{11}	U_{22}	U_{33}	U_{12}	U_{eq}
Sm	1*a*	0	0	0	0.0072(3)	0.0072(3)	0.0069(2)	0.0036(1)	0.0071(2)
Ni	1*d*	1/3	2/3	1/2	0.001(4)	0.001(4)	0.008(6)	0.005(1)	0.0032(3)
As	1*f*	2/3	1/3	1/2	0.009(4)	0.009(4)	0.012(5)	0.004(2)	0.010(3)

Table 8. Main interatomic distances (Å) for SmNiAs.

Sm –	6Ni	3.0612(2)	As –	3Ni	2.3616(2)
	6As	3.0612(2)		6Sm	3.0612(2)
	2Sm	3.8957(4)			
	6Sm	4.0904(3)	Ni –	3As	2.3616(2)
				6Sm	3.0612(2)

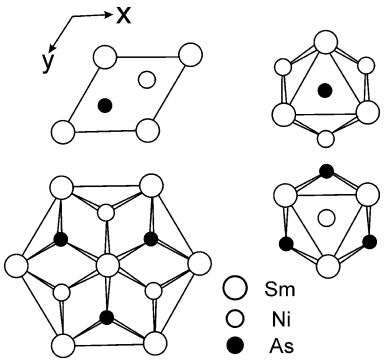

Fig. 4. Projection of the SmNiAs structure on (001). The coordination polyhedra are emphasized.

Crystal structure of SmNiAs

It has been shown for CeNiAs and later for other *Ln*NiAs phases (*Ln* = La to Tm) [3] that these are isotypic with SrPtSb. The structure is derived from the AlB_2 type [35] by ordering the metal atoms in an identical unit cell. There are reports also on a fourfold superstructure along [001] for the equiatomic composition *Ln*NiAs (*Ln* = La to Yb, U) [36] on the basis of X-ray powder data, thus corresponding to the Tb_{1-x}NiP-type structure [37]. In order to solve this discrepancy X-ray single crystal data of SmNiAs were analyzed.

Details of the investigation are listed in Table 6. No additional reflections with regard to the SrPtSb unit cell were detected with different single crystals even with prolonged X-ray exposure. Therefore, the ternary compound SmNiAs does not crystallize in a superstructure of Tb_{1-x}NiP type. The final atomic and displacement parameters are listed in Table 7 and selected bond distances in Table 8.

The samarium atoms occupy the centers of regular hexagonal prisms formed by 6 As and 6 Ni atoms (Fig. 4). Six additional Sm atoms outside the faces of the prism added by two other Sm atoms along [001] complete the coordination number to CN = 20. The CNs for the arsenic and nickel atoms are similar, *i. e.* CN = 9, which corresponds to trigonal prisms of Sm atoms with three additional atoms (either Ni or As) outside the rectangular faces of the prisms.

Discussion

Neither solid solutions based on the binary arsenides nor homogeneity ranges for the ternary arsenides have been observed in the solid-state phase equilibria of the Sm-Ni-As system, similar to the previously investigated La-Ni-As and Ce-Ni-As systems [3]. On the other hand the Sm-Ni-P system is more complicated than the Sm-Ni-As phase diagram, since only six phases have been observed with arsenic instead of eleven with phosphorus [2]. The additional compounds with lower than 33 at. % non-metal content are $SmNi_4P_2$, $Sm_9Ni_{26}P_{12}$, $Sm_{16}Ni_{36}P_{22}$, $Sm_{25}Ni_{49}P_{33}$, and $Sm_{15}Ni_{28}P_{21}$ [1, 2]. These types of compounds are typical only for ternary rare earth phosphides. The structure types of Fe_2P, $Zr_2Fe_{12}P_7$, $Zr_6Ni_{20}P_{13}$, (La, Ce)$_{12}Rh_{30}P_{21}$, $Sm_{20}Ni_{42}P_{31}$, and SrPtSb are common to both ternary systems.

Table 9 contains a compilation of all the lanthanoid nickel arsenides known together with their structural types. Samarium joins the rare earths of the cerium group metals. A trigonal prismatic coordination by metalloid atoms is found with compounds of all lanthanides, La to Yb, whereas an octahedral coordination like in the Zr_2NiAs_2 or $ZrFe_4Si_2$ types structures is restricted to the late rare earths, Gd to Yb, and distorted cubic or antiprismatic coordination like in the $ThCr_2Si_2$ or $CaBe_2Ge_2$ type structures occurs with the early rare earths, La to Sm.

In the Sm-Ni-As system, all ternary phases, $Sm_2Ni_{12}As_7$, $Sm_6Ni_{20}As_{13}$, $Sm_6Ni_{15}As_{10}$, $Sm_{20}Ni_{42}As_{31}$, and SmNiAs, except for $SmNi_2As_2$, exhibit an approximate metal/metalloid ratio of 2. Moreover, they are successive members with $n = 2, 3, 4, 5$, and ∞ of the basic series with hexagonal symmetry having the general formula $R_{n(n-1)}T_{(n+1)(n+2)}X_{n(n+1)+1}$ (R = Zr or rare earth); T = 3d or 4d transition metal; X = P, As). This structural family is characterized by flat hexagonal two-net structures and has been described in different ways [1, 9]. One description is based on the formation of slightly distorted trigonal nets of metalloid atoms in the projection perpendicular to the smallest unit cell direction [9]. Therefore, one can consider the stacking of trigonal prisms formed by metal atoms R and T and centered by the non-metal atoms X. Phosphorus obviously favours to enter these positions, since

Table 9. Ternary lanthanoid nickel arsenides and their structural types.

Compound	Structure type	Y	La	Ce	Pr	Nd	Sm	Eu	Gd	Tb	Dy	Ho	Er	Tm	Yb	Lu	Refs.
Ln_2NiAs_2	Zr_2NiAs_2									■	■	■	■	■	■		[36, 38]
$LnNi_2As_2$	$CaBe_2Ge_2$		■	■	■	■	■										[25, 26]
$LnNi_2As_2$	$ThCr_2Si_2$		■	■	■	■	■	■									[25, 26]
$LnNi_{1.91}As_{1.94}$	$URh_{1.6}As_{1.9}$			■		■											[25, 39]
$LnNiAs$	SrPtSb		■	■	■	■	■		■	■	■	■	■	■			[3, present work]
$Ln_{20}Ni_{42}As_{31}$	$Sm_{20}Ni_{42}P_{31}$		■	■	■	■	■		■	■	■						[3, 5]
$Ln_{13}Ni_{25}As_{19}$	$Tm_{13}Ni_{25}As_{19}$													■	■	■	[40]
$Ln_3Ni_7As_5$	$Ce_3Ni_7As_5$		■	■	■	■	■										[6]
$Ln_{12}Ni_{30}As_{21}$	$Dy_{12}Ni_{30}As_{21}$									■	■						[41]
$Ln_6Ni_{15}As_{10}$	$Tb_6Ni_{15}As_{10}$		■				■	■	■	■	■						[10, present work]
$Ln_6Ni_{20}As_{13}$	$Zr_6Ni_{20}P_{13}$		■	■	■	■	■		■	■	■	■	■				[27]
$Ln_2Ni_{12}As_7$	$Zr_2Fe_{12}P_7$		■		■	■	■		■	■	■	■	■	■	■	■	[28, 29]
$LnNi_5As_3$	$LaCo_5P_3$							■									[42]
$LnNi_5As_3$	$LaNi_5As_3$		■	■													[7]
$LnNi_4As_2$	$ZrFe_4Si_2$		■						■	■	■	■	■	■	■	■	[43, 44]

its covalent radius (1.10 Å) is smaller than that of arsenic (1.18 Å) [33], which may explain the greater number of ternary phosphides. The trigonal prisms are connected only *via* common edges in such a way that no *X*-*X* bonds occur. Hence, *e. g.* the $Sm_6Ni_{15}As_{10}$ structure which corresponds to $n = 4$ in the basic series with two formula units per cell contains two identical blocks centered on the three-fold axes and mutually displaced by $c/2$ (Fig. 3). The *c*-axis is the shortest cell parameter and represents the height of a trigonal prism. The *n* value in the general formula, mentioned above, depends directly on the number of trigonal prisms forming the width of each block. When *n* tends to infinity, *i. e.* in SmNiAs, a net of only trigonal prisms results.

Conclusion

The investigation of the solid-state phase equilibria in the Sm-Ni-As system at 1170 K (0 – 33 at. % Sm) and 770 K (33 – 80 at. % Sm) led to the discovery of six ternary arsenides, among which two phases, $Sm_6Ni_{15}As_{10}$ and SmNiAs, have been structurally studied. All these phases belong to the hexagonal basic structural series formed by the structural types $Zr_2Fe_{12}P_7$ ($n = 2$), $Zr_6Ni_{20}P_{13}$ ($n = 3$), $(La,Ce)_{12}Rh_{30}P_{21}$ ($n = 4$), $Ce_{20}Ni_{42}As_{31}$ ($n = 5$) and SrPtSb-type ($n = \infty$). Additional phases with $5 < n < \infty$ may also be formed like in the phosphide systems [2, 45], however only under varied and specifically controlled preparative conditions.

Acknowledgements

The authors thank J. C. Jegaden and J. Le Lannic (CMEBA, Université de Rennes 1) for their assistance with SEM and EPMA studies, T. Roisnel (CDIFX, Université de Rennes 1) for X-ray single crystal intensity data collection as well as F. Weitzer (University of Vienna) for his assistance during the X-ray powder studies.

[1] Yu. Kuz'ma, S. Chykhrij, in K. A. Gschneider (Jr.), L. Eyring (eds): Handbook on the Physics and Chemistry of Rare Earths, Vol. 23, p. 285, Elsevier, Amsterdam, (1996).
[2] Yu. Kuz'ma, V. Babizhetskyy, S. Oryshchyn, S. Chikhrij, Zhur. Neorg. Khim. **42**, 308 (1997).
[3] V. Babizhetskyy, C. Le Sénéchal, J. Bauer, S. Députier, R. Guérin, J. Alloys Compd. **287**, 174 (1999).
[4] G. Wenski, A. Mewis, Z. Anorg. Allg. Chem. **535**. 110 (1986).
[5] V. Babizhetskyy, C. Le Sénéchal, R. Guérin, O. Isnard, K. Hiebl, Phys. Rev. B. **66**, 014102 (2002).
[6] V. Babizhetskyy, R. Guérin, O. Isnard, K. Hiebl, J. Solid State Chem. **172**, 265 (2003).
[7] V. Babizhetskyy, R. Guérin, A. Simon, Z. Naturforsch. **59b**, 1103 (2004).
[8] Ya. P. Yarmoljuk, L. G. Aksel'rud, Kristallografiya. **28**, 1111 (1983).
[9] J.-Y. Pivan, R. Guérin, J. Solid State Chem. **135**, 218 (1998).
[10] V. Babizhetskyy, K. Hiebl, A. Simon, J. Alloys Compd. **413**, 17 (2006).
[11] COLLECT: KappaCCD software, Nonius BV, Delft, The Netherlands (1998).

[12] Z. Otwinowski, W. Minor, in C. W. Carter (Jr.), R. W. Sweet (eds): Methods in Enzymology, Vol. 276, Academic Press, New York (1997).
[13] A. Altomare, M. C. Burla, M. Camalli, B. Carrozzini, G. L. Cascarano, C. Giacovazzo, A. Guagliardi, A. G. G. Moliterni, G. Polidori, R. Rizzi, Acta Crystallogr. **A32**, 115 (1999).
[14] G. M. Sheldrick, SHELXL-97, Program for Refinement of Crystal Structures, University of Göttingen (1997).
[15] K. Brandenburg, DIAMOND, Version 2.1d (2000).
[16] T. B. Massalski: Binary Alloy Phase Diagrams, 2nd ed., ASM, Materials Park, OH (1990).
[17] P. Villars, L. D. Calvert: Pearson's Handbook of Crystallographic Data for Intermetallic Phases, 2nd ed., ASM, Materials Park, OH (1991).
[18] K. H. J. Buschow, A. S. Van der Goot, J. Less-Common Met. **22**, 419 (1970).
[19] S. Takeda, Y. Kitano, Y. Komura, J. Less-Common Met. **84**, 317 (1982).
[20] A. Ochiai, T. Suzuki, T. Kasuya, J. Magn. Magn. Mater. **52,** 13 (1985).
[21] A. Ochiai, T. Suzuki, T. Kasuya, J. Alloys Compd. **192**, 253 (1993).
[22] A. Yamasaki, A. Sekiyama, S. Imada, M. Tsunekawa, C. Dallera, L. Braicovich, T.-L. Lee, A. Ochiai, S. Suga, J. Phys. Soc. Jpn. **74**, 2538 (2005).
[23] S. Ono, J. Desperault, L. Calvert, J. Taylor, J. Less-Common Met. **22**, 51 (1970).
[24] W. Reiger, E. Parthé, Monatsh. Chem. **100**, 1370 (1969).
[25] E. H. El Ghadraoui, J. Y. Pivan, R. Guérin, O. Pena, J. Padiou, M. Sergent, Mater. Res. Bull. **23**, 1345 (1988).
[26] W. Jeitschko, W. K. Hoffmann, L. J. Terbüchte, J. Less-Common Met. **137**, 133 (1988).
[27] R. Madar, P. Chaudouët, J. P. Sénateur, R. Fruchart, B. Lambert, J. Solid State Chem. **56**, 335 (1985).
[28] W. Jeitschko, B. Jaberg, J. Less-Common Met. **79**, 311 (1981).
[29] E. H. El Ghadraoui, J. Y. Pivan, O. Pena, R. Guérin, P. Bonville, Physica B **163**, 185 (1990).
[30] T. Roisnel, J. Rodriguez-Carvajal, WinPLOTR: a Windows Tool for Powder Diffraction Patterns Analysis, Materials Science Forum, R. Delhez, E. J. Mittenmeijer (eds): Proceedings of the 7th European Powder Diffraction Conference (EPDIC 7), p. 118 (2000).
[31] J. Rodriguez-Carvajal, Phys. B. **192**, 55 (1993).
[32] C. Le Sénéchal, V. Babizhetskyy, S. Députier, J.-Y. Pivan, R. Guérin, J. Solid State Chem. **144**, 277 (1999).
[33] L. Pauling, Nature of the Chemical Bond, 3rd ed., Cornell University Press, Ithaca, NY (1960).
[34] F. Laves, Theory of Alloy Phases, ASM, Cleveland, OH (1956).
[35] W. Hoffman, W. Jäniche, Naturwiss. **23**, 851 (1935).
[36] W. Jeitschko, L. J. Terbüchte, U. Ch. Rodewald, Z. Naturforsch. **56b**, 1281 (2001).
[37] S. Chikhrij, S. Oryshchyn, Yu. Kuz'ma, Zhur. Neorg. Khim. **32**, 1386 (1987).
[38] E. H. El Ghadraoui, J. Y. Pivan, R. Guérin, M. Sergent, Mater. Res. Bull. **23**, 891 (1988).
[39] V. Babizhetskyy, E. Le Für, J. Y. Pivan, R. Guérin, Z. Naturforsch. **57b**, 1359 (2002).
[40] W. Jeitschko, L. J. Terbüchte, U. Ch. Rodewald, Z. Anorg. Allg. Chem. **627**, 2095 (2001).
[41] W. Jeitschko, L. J. Terbüchte, U. Ch. Rodewald, Z. Anorg. Allg. Chem. **627**, 2673 (2001).
[42] H. Probst, A. Mewis, Z. Anorg. Allg. Chem. **597**. 173 (1991).
[43] J. Y. Pivan, R. Guérin, E. H. El Ghadraoui, M. Rafiq, J. Less-Common Met. **153**, 285 (1989).
[44] W. Jeitschko, L. J. Terbüchte, E. J. Reinbold, P. G. Pollmeier, T. Vomhof, J. Less-Common Met. **161**, 125 (1990).
[45] S. Chykhrij, V. Babizhetskyy, S. Orychshyn, L. Aksel'rud, Yu. Kuz'ma, Kristallografija. **38**, 262 (1993)